

Geophysical Research Letters

RESEARCH LETTER

10.1029/2020GL091603

Key Points:

- Summer heat anomalies in the northern hemisphere will become more persistent in the midlatitudes, especially in southern North America where summer weather patterns and associated temperature anomalies are projected to slow-down by more than 45% by the end of the century
- There are robust relationships between Arctic warming at near surface levels and midlatitude weather persistence in observations and models
- Models disagree on the sign of equator-to-pole temperature gradient change during summer, but those models that agree with observations, a warming Arctic, show a stronger trend toward increased persistence over midlatitude land area (−10%)

Supporting Information:

- Supporting Information S1

Correspondence to:

K. Kornhuber,
kk3397@columbia.edu

Citation:

Kornhuber, K., & Tamarin-Brodsky, T. (2021). Future changes in Northern Hemisphere summer weather persistence linked to projected Arctic warming. *Geophysical Research Letters*, 48, e2020GL091603. <https://doi.org/10.1029/2020GL091603>

Received 16 NOV 2020

Accepted 27 DEC 2020

© 2021. American Geophysical Union.
All Rights Reserved.

Future Changes in Northern Hemisphere Summer Weather Persistence Linked to Projected Arctic Warming

Kai Kornhuber^{1,2}  and Talia Tamarin-Brodsky³ 

¹Earth Institute, Columbia University, New York, NY, USA, ²Lamont-Doherty Earth Observatory, Columbia University, New York, NY, USA, ³Department of Meteorology, University of Reading, Reading, UK

Abstract Understanding the response of the large-scale atmospheric circulation to climatic change remains a key challenge. Specifically, changes in the equator-to-pole temperature difference have been suggested to affect the midlatitudes, potentially leading to more persistent extreme weather, but a scientific consensus has not been established so far. Here we quantify summer weather persistence by applying a tracking algorithm to lower tropospheric vorticity and temperature fields to analyze changes in their propagation speeds. We find significant links between slower propagating weather systems and a weaker equator-to-pole temperature difference in observations and models. By end of the century, the propagation of temperature anomalies over midlatitude land is projected to decrease by −3%, regionally strongest in southern North America (−45%) under a high emission scenario (CMIP5 RCP8.5). Even higher decreases are found (−10%, −58%) in models which project a decreasing equator-to-pole temperature difference. Our findings provide evidence that hot summer weather might become longer-lasting, bearing the risk of more persistent heat extremes.

1. Introduction

Global mean temperatures are increasing due to anthropogenic activity, but this warming is not distributed uniformly. Arctic regions are warming at a higher rate than lower latitudes, a phenomenon coined Arctic amplification (AA), with potential impacts on atmospheric circulation and midlatitude weather (Cohen et al., 2020; Overland et al., 2016). Assessing the impact of heterogeneous warming trends on the atmospheric circulation and on the frequency and magnitude on extreme weather events remains a key challenge in climate science (Barnes, 2013; Barnes & Screen, 2015; Francis & Vavrus, 2012; Shepherd, 2015).

In the midlatitudes, surface weather is strongly influenced by the jet-stream, which tends to advect weather systems, as well as their associated warm and cold temperature anomalies eastwards. The midlatitude jet is generally related, through the thermal wind balance, to the equator-to-pole temperature gradient (e.g., Vallis, 2006). The latter is subject to change in recent years, due to the rapid warming of the Arctic, one of the most prominent signals of anthropogenic climate change (Cohen et al., 2014). While there is a general consensus that Arctic warming *can* have an effect on future changes in extreme weather in the midlatitudes, it is currently still debated *if* and *how* these changes will play out under future emission pathways, and whether such effects can be felt today already (Barnes & Screen, 2015; Blackport & Screen, 2020; Cohen et al., 2020). Studies struggle with the relatively short observational time-series of variables such as upper level wind and pressure fields, making it challenging to rule out the signatures of multidecadal variability in observations. Moreover, discrepancies between models and observations still exist, indicating that some of the relevant physical linkages might be underestimated (Schiemann et al., 2020). In addition, the vertical structure of AA is complex and differs seasonally. In contrast to a lower level warming, a cooling trend has been observed in the upper Arctic troposphere (Cohen et al., 2014), while the tropical upper troposphere is warming leading to a temperature gradient increase at higher altitudes. The opposing effects of these observed trends on the midlatitude circulation have been coined a *Tug-of-war* (Shaw & Voigt, 2015): while a decrease in lower level equator-to-pole-temperature gradient would lead to an equatorward shift and a decrease in storm track activity (Coumou et al., 2015), the opposite is expected for an increase in the upper level temperature gradient, possibly balancing out the annual mean changes (Barnes & Screen, 2015; Lee, et al., 2019). In summer, storm tracks have been reported to weaken, consistent with a slow-down of the midlatitudinal zonal winds (Coumou et al., 2015).

Past efforts have put an emphasis on linking a warmer Arctic to the waviness of the midlatitude jet, but no consensus has been reached so far (Blackport & Screen, 2020; Cohen et al., 2020). A number of diagnostic approaches were introduced to quantify circulation changes, but their trends and impacts over the observational time period have been shown to be sensitive to the exact methodology (Barnes, 2013; Francis & Vavrus, 2012; Screen & Simmonds, 2013; Wills et al., 2019), and their relevance for the actual near-surface weather systems was often not assessed. In addition, specific wave patterns of the jet characterized by a hemispheric wavenumber 5 and 7 and associated with severe heatwaves have been reported to become more frequent (Kornhuber et al., 2019; Lee et al., 2017), but a direct link to a warmer arctic has so far remained suggestive (Coumou et al., 2014, 2015). Most studies that aim to relate a warming arctic to midlatitude extreme weather focus on winter climates and cold-spells (Blackport & Screen, 2020; Cohen et al., 2014, 2020), while the effect of a decreasing temperature gradient on summer circulation has received less attention (Coumou et al., 2018; Horton et al., 2015; Mann et al., 2018). This is in spite of the fact that in summer changes in extreme heat waves could act on top of the thermodynamic warming trend, while extreme cold spells in winter might become less severe in future climates (Tamarin-Brodsky et al., 2020). Impacts of extreme heat waves on human health, livestock and agricultural production amplify when persisting for an extended period. As opposed to previous studies, which were primarily focused on the wave disturbances (e.g., derived from geopotential height anomalies (Barnes, 2013; Francis & Vavrus, 2012, 2015) or changes in the persistence of local weather conditions (based on counting of subsequent days of continuous warm-dry or cold-wet episodes (Pfleiderer & Coumou, 2017; Pfleiderer et al., 2019), we introduce a novel approach to quantify the key dynamical characteristics of heat anomalies for the investigation of their future persistence changes. By modifying a cyclone feature-tracking algorithm (Hodges, 1995) and applying it to low-level temperature anomalies (Tamarin-Brodsky et al., 2019, 2020) we are able to quantify the future changes in weather persistence and their relationship to physical drivers such as zonal wind speed and the large-scale temperature gradient, which have been discussed in the context of changes in midlatitude extreme weather. Our analysis aims at tackling the following research questions:

1. What is the relationship between weather persistence, jet speed, and the low-level equator-to-pole temperature gradient?
2. How is local weather persistence projected to change under a high emission scenario and to what extent do models agree?
3. Can projected changes in weather persistence be linked to changes in the equator-to-pole temperature gradient and a weakened jet in models?

In this context, we use the term “*weather*” for the combination of both midlatitude synoptic cyclones and anticyclones, as well as their associated temperature anomalies. Thus, a *slow-down* in their eastward propagation is interpreted as an *increase* in *weather* persistence. In the following sections, we introduce the tracking algorithm, provide a short introduction to the theoretical considerations and the datasets used (Section 2). We then provide evidence that weather persistence is significantly linked to zonal wind strength and the equator-to-pole temperature gradient in reanalysis data and models and show that the spread in projected weather persistence corresponds to projected changes in polar warming (Section 3). These results are discussed and put into context in Section 4.

2. Data, Methods, and Theoretical Considerations

2.1. Lagrangian Feature-Tracking of Vorticity- and Temperature Anomalies

Feature-tracking is a widely used technique to diagnose the specific dynamical properties (e.g., propagation speed) of weather systems. We identify and track vorticity and temperature anomalies using the tracking algorithm of (Hodges, 1995), which allows for a quantification of their tracks, propagation speeds, and the intensity of the tracked anomalies. As we are interested in the near-surface conditions during summer, we focus on the 850 hPa level anticyclones and positive temperature anomalies, which are more relevant for heat waves (but similar qualitative results are obtained for cyclones and negative temperature anomalies, (see Figure S1). In the following, we provide an overview of the tracking algorithm, but refer the interested reader to (Hodges, 1995) for a more comprehensive description of the technical details. Anticyclones are identified as positive anomalies in the relative vorticity field, which is computed using the zonal and

meridional wind velocities on a 6-hourly time resolution. Anomalies are determined by subtracting a background state, and features are identified as localized maxima/minima of the anomaly field. The background state is defined as the climatology of the large-scale flow (wavenumbers smaller than 5). For the tracking of temperature anomalies, we remove the diurnal cycle by subtracting climatologies on a 6-hourly time resolution for each time-step (i.e., averaging over all considered years for each 6-hourly time-step separately). For both vorticity and temperature, anomalies are smoothed to a T42 grid (approximately 2.8° resolution) before the tracking, to avoid small-scale noise. The centers of the features are then tracked by performing a nearest neighbor method between time-steps (but ensuring the smoothness of the tracks by adding restrictions on their propagation direction and speeds [Hodges, 1999]). As is typically done for vorticity, only features that last for more than two days and propagate distances larger than 1,000 km are considered for further analysis. For temperature anomalies, this condition is relaxed, so that stationary perturbations like heat waves can be detected. The tracking algorithm not only provides us with the tracks of the features (position at every time-step), but also with spatial maps of averaged statistics such as their mean propagation speeds. The statistics are calculated by extrapolating the values along the tracks from all the features aggregated over a season, using locally defined spherical kernel estimator, which constitute a type of distance weighted statistical estimator (Hodges, 1995).

2.2. Data

The analysis is based on ERA-Interim reanalysis data (Dee et al., 2011) and output from the coupled model intercomparison project (CMIP5) (Taylor et al., 2012) for Northern Hemisphere summer months (June–August, JJA). Temperature and zonal wind fields are analyzed on the 850, 500 and 250 hPa levels on a 2.5×2.5 grid. For ERA-interim we investigate the period 1981–2014. CMIP5-data is based on data from 20 models (see model list in Figure 4) from the representative concentration pathway 8.5 (RCP8.5) emissions scenario and historical simulations, using the r1i1p1 ensemble member. A period of 24 years is used in the historical (1981–2004) runs and 19 years in the projected (2081–2099) runs. The meridional temperature gradient dT/dy was approximated by subtracting the zonally averaged temperature at high latitudes (65°N – 90°N) from the midlatitudinal belt (30°N – 50°N) and dividing by 40° , following the approach taken in other studies (Blackport & Screen, 2020). The zonally averaged values of the zonal wind U , the meridional temperature gradient dT/dy , and the zonal propagation speeds of anticyclones (c_{cx}) and warm temperature anomalies (c_{tx}) were linearly detrended, to avoid spurious correlations. With the exception of U at the 250 hPa level, all variables investigated exhibited a decreasing (although nonsignificant) trend over the investigated period (1979–2014) (Figures S2 and S11). Meridional averages were computed over the midlatitude belt (40°N – 70°N), though results are found to be insensitive to the exact choice of latitudinal boundaries. The analysis presented here is focused on the zonal components of c_c and c_t , as those are more directly linked to U , and because the zonal propagation speeds are found to dominate the absolute value of the phase speed. This is demonstrated in Figures S8 and S9, showing changes in the total propagation speeds and in the meridional propagation speed of anticyclones (c_{cy}) and positive temperature anomalies (c_{ty}), respectively.

2.3. Theoretical Considerations for the Eastward Propagation of Weather Patterns

To the extent that extratropical weather systems can be represented as free Rossby waves, the relation between the zonal propagation speed of weather systems c_{cx} and the zonal mean flow U can be investigated by considering the linearized vorticity equation. In the simplest case of freely propagating Rossby waves on a beta plane, a 2D nondivergent flow and a zonally and meridionally uniform flow U , the dispersion relation and associated zonal phase speed of Rossby waves c_x (e.g., Vallis, 2006) are given by:

$$c_x = U - \beta / (k^2 + l^2) \quad (1)$$

where k and l are the zonal and meridional wavenumbers, respectively. Equation 1 suggests that the zonal phase speed c_x of atmospheric Rossby waves is proportional to the mean zonal flow U minus the westward self-propagation of the waves (the second term on the right hand side of [1]). Hence, assuming β , k , and l

remain constant, we can expect changes in c_x to follow changes in U (although the relevant wavenumbers k and l can generally change too). In a more realistic case (e.g., for Rossby waves propagating on a jet), β on the right hand side of Equation 1 should be replaced with the mean potential vorticity gradient, which could depend on U and the meridional temperature gradient dT / dy as well. Hence, the westward self-propagation of the waves could also change in response to a change in U or dT / dy . Nonetheless, the results presented in the Section 3 suggest that the changes in the propagation speeds indeed correlate well with the changes in U .

Assuming that the eastward propagation velocity of vorticity c_{cx} and temperature anomalies c_{tx} follows the troughs and ridges of propagating Rossby waves (i.e., $c_x \equiv c_{cx}$, $c_x \equiv c_{tx}$), we can thus also expect:

$$c_{cx} \sim U; c_{tx} \sim U. \quad (2)$$

Above the boundary layer, the vertical shear of the zonal mean flow dU / dp can be further related to the equator-to-pole temperature gradient dT/dy by the thermal wind balance:

$$dU / dp = R / f p (dT / dy), \quad (3)$$

where p is the pressure, R is the gas constant and f is the Coriolis parameter. When integrating Equation 3 from the surface to 500 hPa, it follows that U on the 500 hPa level is proportional to the vertical average of the equator-to-pole temperature gradient dT / dy from the surface to 500 hPa (assuming that the mean flow is zero at the surface):

$$U_{500} \sim \overline{dT / dy}. \quad (4)$$

For simplicity, we assume $\overline{dT / dy} \equiv dT / dy$ at the 850 hPa level, which we chose as an equivalent level to its vertical average. The results are not affected qualitatively (i.e., relationships are still statistically significant) by the exact choice of the level as long as it in the lower troposphere (compare Figures S3–S5, that show correlations on 850, 500, and 250 hPa, respectively). Relating the linear relationship expressed in [4] and [2] suggests that:

$$C_{cx} \sim \frac{dT}{dy} \text{ and } C_{tx} \sim \frac{dT}{dy}, \quad (5)$$

an approximately linear relationship between the equator-to-pole temperature gradient and weather persistence in the midlatitude. In the following section we investigate to what extent these crude approximations are justified, and whether such linear relationships between dT / dy , U , c_{cx} , and c_{tx} , as suggested by (2) and (5), can be indeed found in reanalysis and model data (Figures 2 and 3).

3. Results

The most impactful heatwaves of the past decades were not only characterized by extreme temperatures, but also by their unusual persistence. To showcase the temperature anomaly tracking algorithm and its output, we provide anomaly tracks detected during two major Northern Hemisphere heatwaves (Figure 1): the 2003 heatwave in western Europe (Figures 1a and 1b) and the 2010 heatwave over the larger Moscow area (Figures 1c and 1d), both associated with amplified mortality, harvest failures, wildfires, and damages to infrastructure and economy (Kornhuber et al., 2016, 2020; Lau & Kim, 2012). These events were not only extreme in their intensity but also unusual in their persistence. The eastward propagation speed c_{tx} and maximum intensity I_{\max} (defined as the highest temperature anomaly during the life time of a track) and life time of all temperature anomaly tracks detected over central Europe (Figure 1a) and the larger Moscow region (Figure 1c) during June–August (JJA) are provided in Figures 1b and 1d. For both regions, three of the five most intense tracks were detected in 2003 and 2010 for central Europe and Moscow, respectively, and those tracks were also among the slowest tracks detected. The tracking algorithm successfully captures both the extreme intensity and the exceptional persistence of these two events, which gives confidence in its utility for examining the potential changes in the persistence of such extreme events.

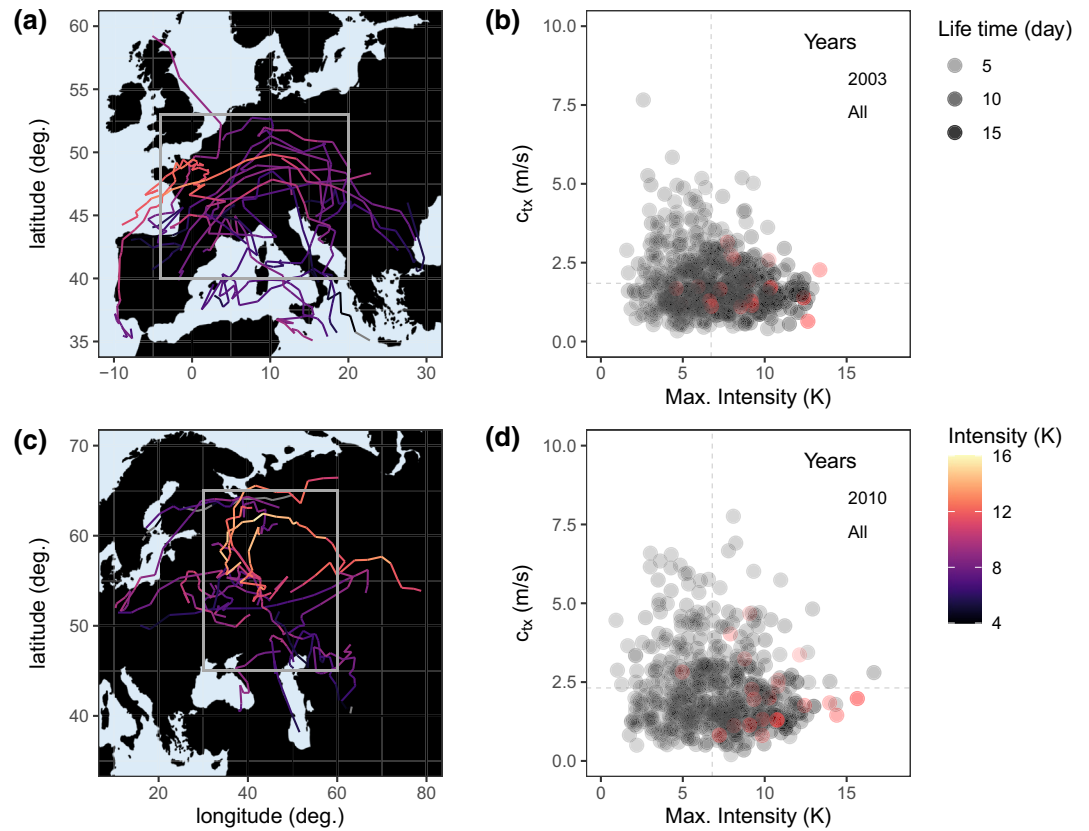


Figure 1. Tracking positive temperature anomalies in ERA-I reanalysis data. Tracks of positive temperature anomalies in (a and b) Europe (-4°W – 20°E ; 40°N – 53°N) and (c and d) Russia (30°E – 60°E ; 45°N – 65°N , also see boxes in Figure 4a) during summer (JJA, 1981–2014). (a and c) Trajectories of all tracks that crossed central Europe (Russia) in JJA 2003 (2010), with color denoting the intensity of their temperature anomaly in Kelvin. (b and d) The mean zonal propagation speed of each warm temperature anomaly (c_{tx}) that crossed the region, plotted against their maximum intensity reached along the track within their lifetime. The life time in days of each track (time spent within the region) is depicted by the gray shading, vertical (horizontal) gray dashed lines provide the average maximum intensity (c_{tx}). Years 2003 and 2010 are shown in red for central Europe and Russia, respectively. JJA, June–August.

3.1. A Relation Between Weather Persistence and the Meridional Temperature Gradient

To investigate the role of large scale climatic conditions, such as the zonal mean zonal wind U and the equator-to-pole temperature gradient dT/dy in weather persistence, we plot c_{cx} , c_{tx} (850 hPa), U (500 hPa), and dT/dy (850 hPa) against each other and perform a linear regression (Figure 2). We find significant linear relationships between dT/dy and all other measures, namely U , c_{cx} , and c_{tx} (Figures 2a–2c), in agreement with the idealized relationships derived in Section 2.4. The described variance is highest for U ($R^2 = 0.37$) and lowest for c_{tx} ($R^2 = 0.17$). Regressing U directly to c_{cx} and c_{tx} yields significant correlations with highest described variance of $R^2 = 0.55$ for U and c_{cx} highlighting the strong ties between zonal winds and storm-tracks (Figures 2d–2f), and $R^2 = 0.32$ for U and c_{tx} . In addition, a statistically significant relationship is found when regressing c_{cx} and c_{tx} although the described variance is lower ($R^2 = 0.18$) compared to the regression of U and c_{tx} suggesting that the eastward propagation of temperature anomalies is more strongly related to the zonal winds directly rather than to the eastward propagation of cyclones and anticyclones. Finally, we note that while significant links are found between U , c_{cx} , c_{tx} and the lower-level temperature gradients dT/dy , no such correlations are found for upper-levels at 250 hPa (Figures S3–S5). This suggests that changes in the upper level temperature gradients in summer are less important for the low level temperature persistence.

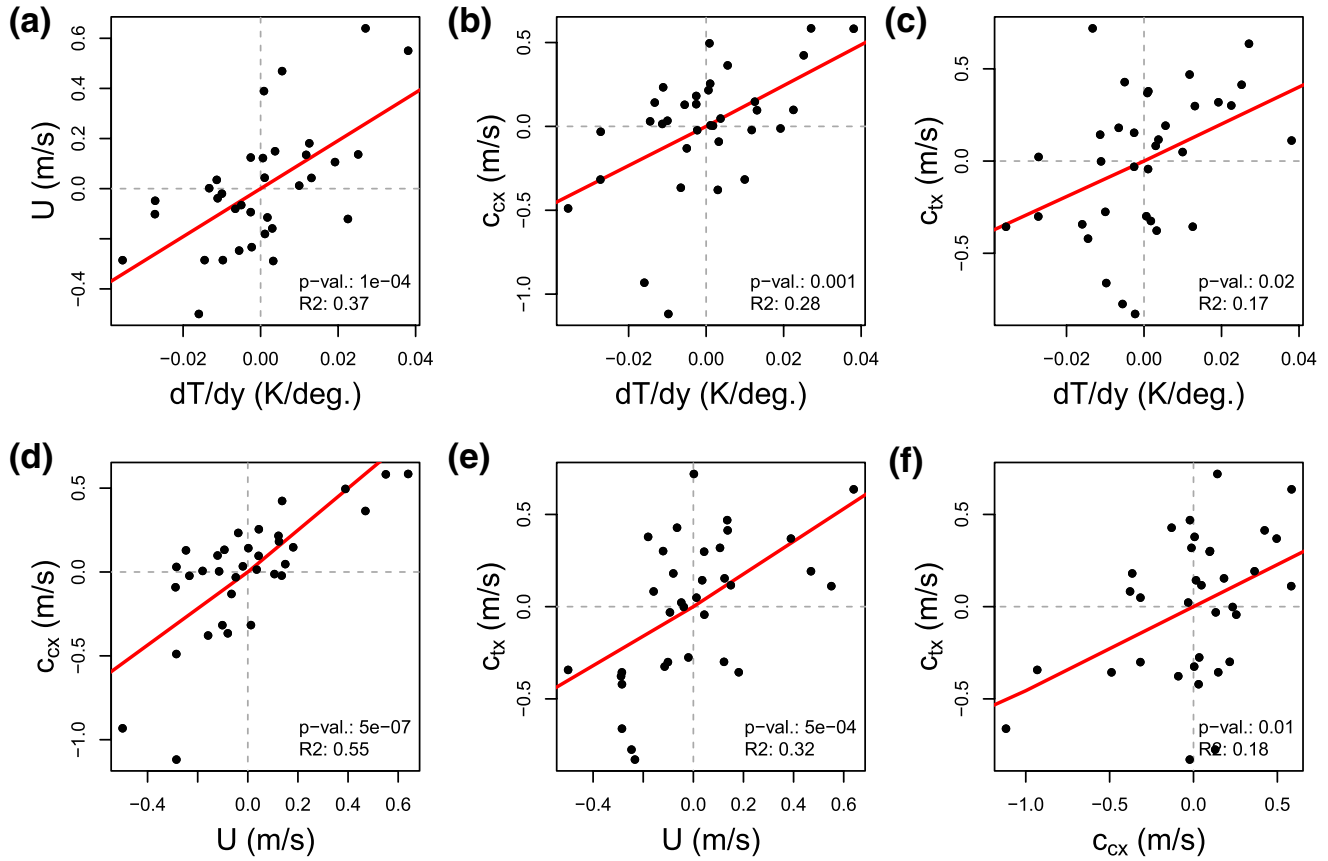


Figure 2. Linear regression of meridional temperature gradient dT / dy (850 hPa), zonal wind U (500 hPa), and propagation speeds of anticyclones c_{cx} and positive temperature anomalies c_{tx} (both 850 hPa) in ERA-I reanalysis data (1981–2014) during summer (JJA). The correlation between seasonally averaged zonal mean meridional temperature gradient and (a) zonal wind U , (b) zonal velocity of anticyclones (c_{cx}), and (c) zonal velocity of positive temperature anomalies (c_{tx}) in the midlatitudes (40–70°N). Panels (d–f) show the analogue for correlations between zonal mean wind U and zonal velocity of (d) anticyclones (c_{cx}), and (e) positive temperature anomalies (c_{tx}), and (f) the correlation between the zonal velocity of cyclones (c_{cx}) and positive temperature anomalies (c_{tx}). A linear fit is shown in red, p -values and R^2 are provided in the lower right corner. All four metrics are significantly correlated. Similar results are obtained for cyclones and negative (cold) temperature anomalies (Figure S1). JJA, June–August.

3.2. Uncertainty in Future Changes of Weather Persistence Linked to Projected Arctic Warming

The existence of decadal fluctuations in the atmospheric circulation makes it challenging to distinguish a forced response from the background signal over the relatively short period for which reliable observational time series are available. To assess the potential future changes in the dynamical characteristics of temperature anomalies, we apply the tracking algorithm to 20 models of the CMIP5 ensemble (see Methods for details). Tracks are assessed on historic (*hist*, 1981–2004) and future projections in a high emission scenario (*rcp8.5*, 2081–2099). In order to analyze the modeled interrelationships and model spread, we investigate the projected changes in the zonally averaged $\Delta dT / dy$, ΔU , Δc_{cx} , and Δc_{tx} in JJA (Figure 3). In agreement with Barnes and Polvani (2015), who investigated changes of U and the meridional temperature gradient over the North Atlantic, we find that the model spread in $\Delta dT / dy$ describes the model spread in ΔU well (p -value < 0.05), with a R^2 value of 0.28 (Figure 3a). The correlations between $\Delta dT / dy$ and Δc_{cx} , and Δc_{tx} are also both found to be significant at a 95% confidence level with R^2 values of 0.71 and 0.52 respectively, (Figures 3b and 3c). In agreement with the significant correlations found in reanalysis data, ΔU with Δc_{cx} and Δc_{tx} as well as Δc_{cx} with Δc_{tx} are found to be significantly related in models (Figures 3d–3f), with highest values of described variance for Δc_{cx} with Δc_{tx} ($R^2 = 0.72$). Thus, models that project an increase of dT / dy in the midlatitudes also tend to project an increase of U , c_{cx} , and c_{tx} while models that project a decrease in dT / dy tend to project a decrease of U , c_{cx} , and c_{tx} , highlighting the considerable linkages between these four variables.

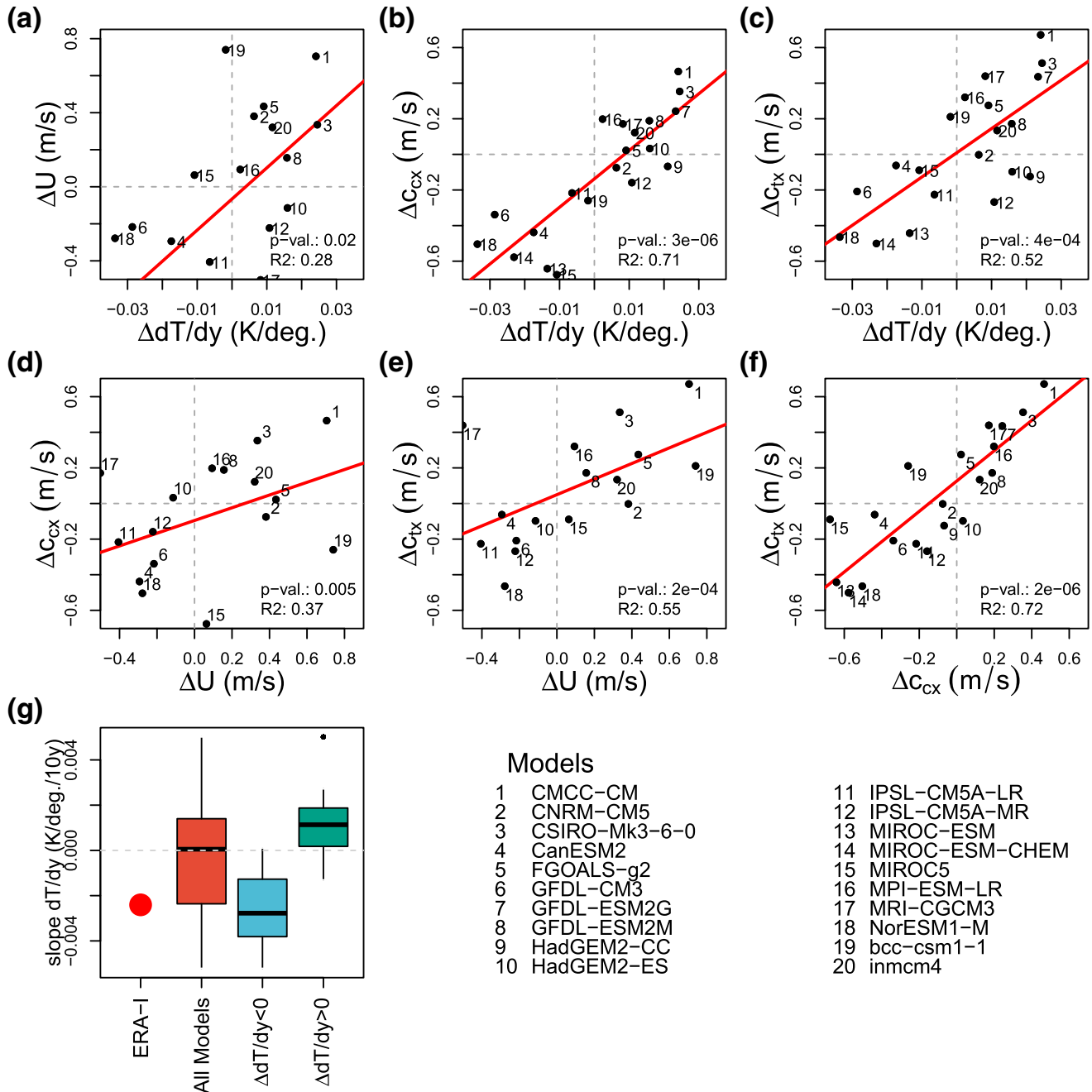


Figure 3. Linear regression of projected changes in CMIP5-models (historical, 1981–2004 vs. RCP8.5, 2081–2099) in the meridional temperature gradient $\Delta dT/dy$ (850 hPa), zonal wind ΔU (500 hPa), and propagation speeds of anticyclones Δc_{cx} and temperature anomalies Δc_{tx} in summer (JJA). The correlation between projected changes in seasonally averaged zonal mean meridional temperature gradient $\Delta dT/dy$ and (a) zonal mean winds ΔU (b) zonal velocity of anticyclones (Δc_{cx}) and (c) zonal velocity of temperature anomalies (Δc_{tx}) in the midlatitudes (40°N–70°N) during summer (JJA), for all CMIP5 models provided in the list. Panels d–f show a similar analysis but for correlations between changes in the zonal mean wind U and the zonal velocity of (d) anticyclones (Δc_{cx}), and (e) warm temperature anomalies (Δc_{tx}), and (f) the correlation between the changes in zonal velocity of anticyclones (Δc_{cx}) and warm temperature anomalies (Δc_{tx}). (g) Change of dT/dy taken from a linear regression over the years 1981–2018 over 10 years, for the reanalysis data and for the two subsets of models projecting either a decreasing or an increasing dT/dy in the future (2081–2099). JJA, June–August.

Assessing changes in $\Delta dT/dy$ shows that the models do not agree on the sign of the projected future changes in summer (Figures 3a–3c). To further investigate this, the models are split into two groups according to their future projection of the meridional temperature gradient ($\Delta dT/dy > 0$, $\Delta dT/dy < 0$), in the spirit of a story-line approach (Zappa & Shepherd, 2017). Each group makes up about half of the total number of

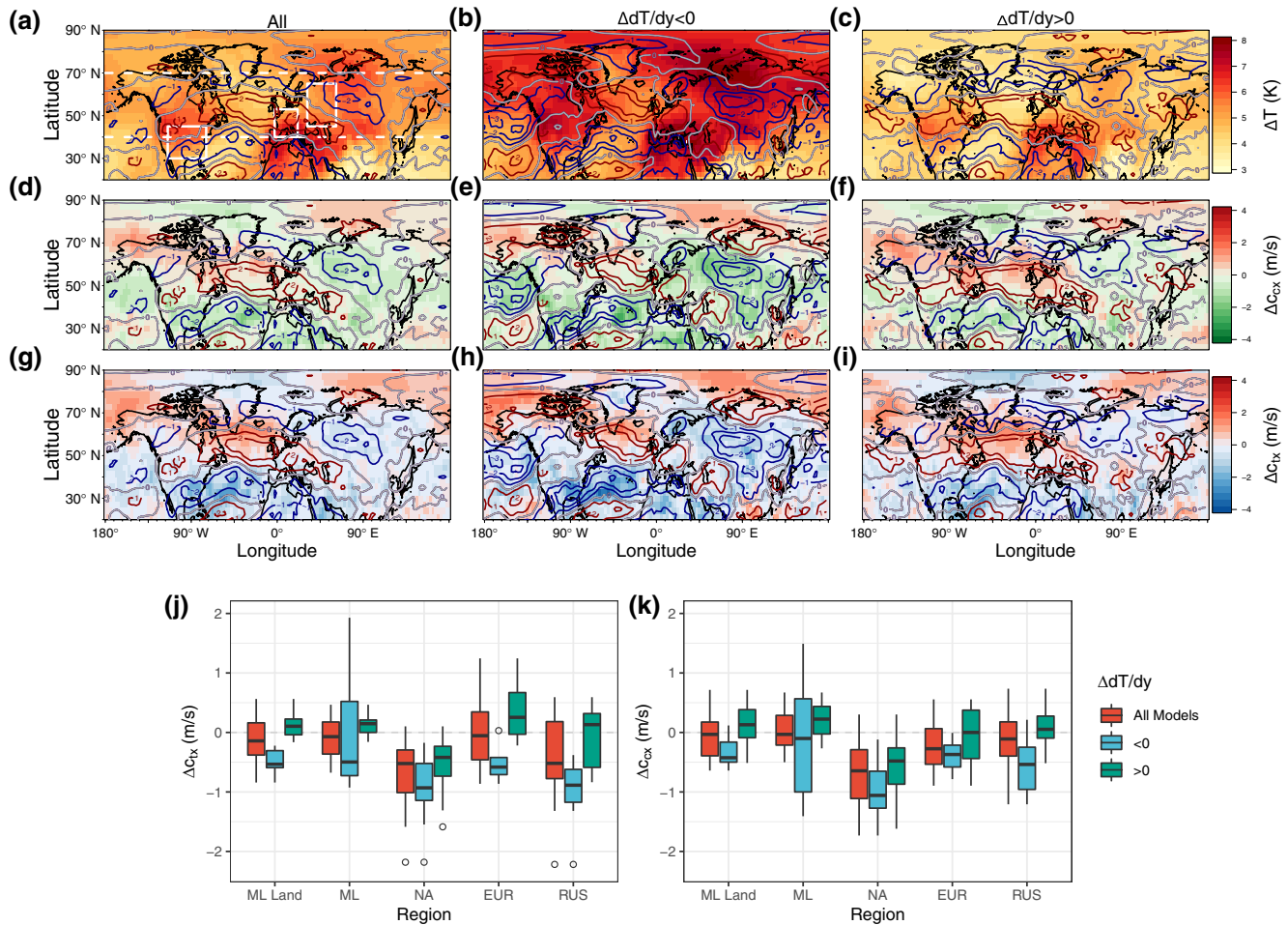


Figure 4. Spatial patterns of projected changes in CMIP5 (historical, 1981–2004 vs. RCP8.5, 2081–2099) in summer (JJA) temperature (850 hPa) (a–c), and the eastward propagation speeds of anticyclones (c_{cx}) (d–f) and temperature anomalies (c_{tx}) (g–i) in CMIP5 models, and their relation to projected changes in the equator-to-pole temperature gradient $\Delta dT / dy$. Projected changes in 850 hPa temperature (filled contours) for (a) all models, (b) models that project a decreasing temperature gradient $\Delta dT / dy < 0$, and (c) models that project an increase in temperature gradient $\Delta dT / dy > 0$. (d–f) Are analogs plots but for the zonal propagation speed of anticyclones (c_{cx}) and (g–i) for warm temperature anomalies (c_{tx}), respectively. In all panels, changes in the zonal winds U at the 500 hPa level are shown by the line contours, with positive (negative) anomalies in red (blue), the zero-contour in gray, and contour distance of 1 ms^{-1} . (j and k) Boxplot showing the regional distributions of the changes in the zonal propagation speed of (j) warm temperature anomalies (c_{tx}) and (k) anticyclones (c_{cx}) across models, for: the midlatitudinal land area (ML Land), midlatitudes (ML), south North American (NA), central Europe (EUR), and Russia (RUS) (see corresponding boxes in panel a). For a depiction of model agreement on sign of change per grid point see Figure S7. JJA, June–August.

investigated models (see list in Figure 3): 12 project an increasing dT/dy under a future high emission scenario, while 8 project a decreasing dT/dy . Combining model data from historical runs (1980–2004) with the first 14 years from the rcp8.5 experiments (2005–2018) allows us to calculate the modeled change in dT/dy and validate the model's performance by comparing the slope m to the changes in reanalysis data over the same time-period (Figure 3g). While the multimodel average suggests only little change ($m = -0.0003 \text{ K/deg/10 years}$), we find that models projecting a decrease in dT/dy by the end of the century have been considerably closer ($-0.0026 \text{ K/deg/10 years}$) to the values based on reanalysis ($-0.0023 \text{ K/deg/10 years}$) for the same years, compared to models that suggest an increasing gradient in summer ($0.0012 \text{ K/deg/10 years}$).

3.3. The Projected Increase of Midlatitude Summer Weather Persistence

Regional patterns of future weather persistence relate to projected changes in the equator-to-pole temperature difference in models. In the spirit of a storyline approach, we classify the models by their future projection of dT / dy and investigate the spatial patterns of Δc_{cx} and Δc_{tx} for models that show increasing and

decreasing trends separately, in addition to a multimodel mean (Figure 4). A mean warming is found for the multimodel mean, but models that predict a decreasing temperature gradient tend to be generally much warmer compared to models that project an increasing temperature gradient (Figures 4a–4c). Land areas and the Mediterranean are hotspots for future warming in all three cases, but an amplified warming at higher latitudes is only projected for the $\Delta dT / dy < 0$ subset, as expected (Figure 4b). Multimodel mean fields of Δc_{cx} show a slow-down across most of the midlatitude land areas and a northward shift in U over the North Atlantic, in agreement with earlier studies (Butler et al., 2010), while U over the Pacific is found to be less affected (Figure 4d). We find a robust signal of decreasing Δc_{cx} over land area when analyzing $\Delta dT / dy < 0$ models only (Figure 4e), compared to $\Delta dT / dy > 0$ models (Figure 4f). The poleward shift in U over the North Atlantic is projected to increase Δc_{cx} in the northern North Atlantic, which is the only region in the midlatitude that projects a robust increase in c_{cx} in all three cases (Figures 4d–4f). Strongest differences between the two subsets are found in the midlatitudes for western Europe. There, an increase in c_{cx} is projected for $\Delta dT / dy > 0$ models, consistent with a strengthening and northward shift of U over the North Atlantic into the western European land-areas (Figure 4f). In contrast, models that project $\Delta dT / dy < 0$, project mainly a weakening of Δc_{cx} and U (Figure 4e). These contrasting signals are also observed on zonal averages of upper level U (Figure S10). Similarly, c_{tx} is projected to decrease in the multimodel mean over the southern North Atlantic region, where U is weakening most strongly, and over southern North America, the Mediterranean, and central Eurasia (Figure 4g). This pattern remains largely unchanged in the $\Delta dT / dy < 0$ subset (Figure 4h), although patterns of weakening c_{tx} over Europe and Eurasia are less robust. Overall, a decrease in c_{tx} is projected over land areas in models that project a decrease in $\Delta dT / dy < 0$, especially in the midlatitudes, and the northern North-Atlantic Ocean basin is the only midlatitude region where weather persistence is not projected to increase.

Quantifying projected changes of c_{cx} and c_{tx} over specific regions (Figures 4j and 4k and Table S1), we find that the model agreement is strongest over southern North America, the entry region of the North Atlantic stormtrack. The decrease in propagation velocity is projected for the multimodel mean ($\Delta c_{tx} = -47\%$, $\Delta c_{tx} = -45\%$) and for both subsets ($\Delta dT / dy > 0$: $\Delta c_{cx} = -38\%$, $\Delta c_{tx} = -41\%$; $\Delta dT / dy < 0$: $\Delta c_{cx} = -58\%$, $\Delta c_{tx} = -51\%$), and is probably due to the projected poleward shift of the North-Atlantic stormtracks and the decrease of U in this region (Barnes & Polvani, 2013), which has been linked to the expansion of the Hadley Cell (Yin, 2005). A moderate agreement between models is found over Russia, where the multimodel mean ($c_{cx} = -14\%$, $c_{tx} = -6\%$) and both subsets show an averaged decrease but with magnitudes that differ in strength $\Delta dT / dy > 0$: $\Delta c_{cx} = -3\%$, $\Delta c_{tx} = 1\%$; $\Delta dT / dy < 0$: $\Delta c_{cx} = -32\%$, $\Delta c_{tx} = -16\%$), while only a poor agreement is found over Europe, where subsets strongly disagree on the sign of the projection, highlighting the importance of North Atlantic circulation for European weather.

While the multimodel mean suggests small or no changes in future propagation speeds over Europe ($c_{cx} = -1\%$, $c_{tx} = -6\%$), the $\Delta dT / dy < 0$ subset projects a decrease ($\Delta c_{cx} = -11\%$, $\Delta c_{tx} = -10\%$), in contrast to the $\Delta dT / dy > 0$ subset which suggests an increase in c_{cx} ($\Delta c_{cx} = 6\%$, $\Delta c_{tx} = -3\%$). Overall, c_{cx} is projected to slow down in the midlatitudes in the multimodel mean ($\Delta c_{cx} = -2\%$, $\Delta c_{tx} = 0.1\%$). Here, negative changes over land-area ($\Delta c_{cx} = -3\%$, $\Delta c_{tx} = -2\%$) are canceled out by increases over the Atlantic, with propagation further decreasing ($\Delta c_{cx} = -11\%$, $\Delta c_{tx} = -8\%$) when considering only models that suggest a weakening in future equator-to-pole temperature difference. These results suggest that summer weather might become longer-lasting in the future, bearing the risk of more persistent hot extremes across midlatitude land area, especially over southern North America, where model agreement is most robust.

4. Discussion and Conclusions

In this study, we take a novel approach to investigate weather persistence, by applying a tracking algorithm on vorticity and temperature fields in observations and climate models. We find a slow-down of weather systems and associated surface weather conditions during summer over vast midlatitude land areas projected by the end of the century in a high-emission scenario (Figure 4). Robust links of a decrease in lower- to midlevel tropospheric meridional temperature gradient dT / dy related to AA and a slowdown of U are found in agreement with other studies (Chemke & Polvani, 2020; Coumou et al., 2015), following a linear relationship as suggested by the thermal wind balance (Figure 2a). In addition we show that the eastward

propagation of weather systems c_{cx} and their associated temperature anomalies c_{tx} significantly correlate with U and dT/dy , in agreement with idealized theoretical considerations based on linear Rossby wave theory (Figure 2). Our results imply that summers with warmer temperatures in the Arctic could feature more persistent, slower-moving weather patterns and surface temperature in the midlatitude. In contrast, we find that upper tropospheric temperature gradients to be unrelated to weather persistence as given by a slow-down of the eastward propagation c_{cx} and c_{tx} (Figures S3–S6).

It is important to note that no straightforward causal arguments can be made based on the regression analysis presented here. Given that midlatitude weather systems also transfer heat poleward, more persistent weather could also increase the transport of heat into higher latitudes (Perlwitz et al., 2015; Screen et al., 2012), thus contributing to AA in addition to contributions from, for example, albedo changes due to diminishing sea ice (Screen & Simmonds, 2010). Future studies are needed to further investigate the complex causal pathways on seasonal and subseasonal timescales, which likely point in both directions and differ in magnitude, depending on the background-state conditions.

Large uncertainties in the atmospheric dynamic response to greenhouse-gas emissions remains a key challenge when assessing future extreme weather risk (Overland et al., 2016; Shepherd, 2014). We find that the models disagree on the sign of the equator-to-pole temperature gradient change during summer, but provide evidence that the magnitude of projected Arctic warming is linked to the model spread of future weather persistence (Figure 3). However, by validating the model's performance against the observational data, we find that models projecting a weakening gradient have been more accurate in reproducing past changes, and are thus potentially more reliable for future projections (Figure 4). These models project an increase in weather persistence across the midlatitudes (Table S1), with strongest signals over land-area (−8%), specifically in the South-western United States (−51%) where a slowdown is further enhanced by the poleward shift of the Atlantic stormtrack (Barnes & Polvani, 2013; Yin, 2005). Future work is needed to assess why models disagree on the sign of such a fundamental measure, a suggested way forward being process-based model assessment using causality methods (Nowack et al., 2020) and multimodel large ensemble archives (Deser et al., 2020). Recently reported improvements in blocking characteristics in CMIP6 ensemble might spark hope that models are indeed becoming more reliable in their projections of the atmospheric circulation (Schiemann et al., 2020).

Clearly, the atmospheric circulation is not the sole driver of persistent summer weather in the midlatitudes. Previous studies have shown that extreme heatwaves such as the 2003 and 2010 heatwaves can only be understood when incorporating land-atmosphere feedbacks. Specifically, the lack of evaporative cooling in years of low soil-moisture in spring has been shown to be important for persistent surface extremes, often exceeding the importance of the atmosphere (Horton et al., 2016; Mueller & Seneviratne, 2012). Given that models projecting a stronger AA are also generally warmer (Figure 4), it is possible that in addition to the dynamical factors, land-atmosphere interactions are also contributing to the future slow-down of summer weather patterns and an increase of weather persistence in these models.

While consensus on atmospheric circulation changes in the NH has not been accomplished (Blackport & Screen, 2020; Cohen et al., 2020), this study provides further evidence that future changes in summer weather persistence are related to circulation changes (Chemke & Polvani, 2020; Coumou et al., 2018; Kornhuber et al., 2019; Pfleiderer et al., 2019), suggesting robust links to a warming Arctic (Chemke & Polvani, 2020). Given that models also project robust increases in the magnitude of warm temperature anomalies in some regions relative to an already warming mean temperature (22), the potential combination of increased persistence and hotter extremes can be especially hazardous. Improving our understanding of the projected circulation changes and the regional surface-feedbacks is therefore of crucial importance, especially for regions like the European sector, where the models currently disagree on the sign of the response.

Data Availability Statement

The data used for this study are publicly available and can be obtained from the ECMWF website (ERA-interim Reanalysis: <https://apps.ecmwf.int/datasets/data/interim-full-daily/levtype=sfc/>) and from the WCRP (CMIP5-data: <https://esgf-node.llnl.gov/projects/cmip5/>).

Acknowledgments

Kai Kornhuber and Talia Tamarin-Brodsky are thankful for the valuable input of two anonymous reviewers. Kai Kornhuber was partially supported by the NSF project NSF AGS-1934358.

References

- Barnes, E. A. (2013). Revisiting the evidence linking arctic amplification to extreme weather in midlatitudes. *Geophysical Research Letters*, 40(17), 4734–4739. <https://doi.org/10.1002/grl.50880>
- Barnes, E. A., & Lorenzo, P. (2013). Response of the midlatitude jets, and of their variability, to increased greenhouse gases in the CMIP5 models. *Journal of Climate*, 26(18), 7117–7135. <https://doi.org/10.1175/JCLI-D-12-00536.1>
- Barnes, E. A., & Screen, J. A. (2015). The impact of arctic warming on the midlatitude jet-stream: Can it? Has it? Will it? *Wiley Interdisciplinary Reviews: Climate Change*, 6(3), 277–286. <http://doi.wiley.com/10.1002/wcc.337>
- Blackport, R., & Screen, J. A. (2020). Insignificant effect of arctic amplification on the amplitude of midlatitude atmospheric waves. *Science Advances*, 6(8), 277–286. <https://doi.org/10.1126/sciadv.aay2880>
- Butler, A. H., Thompson, D. W. J., & Ross, H. (2010). The steady-state atmospheric circulation response to climate change-like thermal forcing in a simple general circulation model. *Journal of Climate*, 23(13), 3474–3496. <https://doi.org/10.1175/2010JCLI3228.1>
- Chemke, R., & Polvani, L. M. (2020). Linking midlatitudes eddy heat flux trends and polar amplification. *Npj Climate and Atmospheric Science*, 3(1), 1–8. <https://doi.org/10.1038/s41612-020-0111-7>
- Cohen, J., Screen, J. A., Furtado, J. C., Barlow, M., Whittleston, D., Coumou, D., et al. (2014). Recent arctic amplification and extreme mid-latitude weather. *Nature Geoscience*, 7(9), 627–637. <https://doi.org/10.1038/ngeo2234>
- Cohen, J., Zhang, X., Francis, J., Jung, T., Kwok, R., Overland, J., et al. (2020). Divergent consensus on arctic amplification influence on midlatitude severe winter weather. *Nature Climate Change*, 10(1), 20–29. <https://doi.org/10.1038/s41558-019-0662-y>
- Coumou, D., Di Capua, G., Vavrus, S., Wang, L., & Wang, S. (2018). The influence of arctic amplification on mid-latitude summer circulation. *Nature Communications*, 9(1), 2959. <https://doi.org/10.1038/s41467-018-05256-8>
- Coumou, D., Lehmann, J., & Beckmann, J. (2015). The weakening summer circulation in the northern hemisphere mid-latitudes. *Science*, 348(6232), 324–327. <https://doi.org/10.1126/science.1261768>
- Coumou, D., Petoukhov, V., Rahmstorf, S., Petri, S., & Schellnhuber, H. J. (2014). Quasi-resonant circulation regimes and hemispheric synchronization of extreme weather in boreal summer. *Proceedings of the National Academy of Sciences of the United States of America*, 111(34), 12331–12336. <https://doi.org/10.1073/pnas.1412797111>
- Dee, D. P., Uppala, S. M., Simmons, A. J., Berrisford, P., Poli, P., Kobayashi, S., et al. (2011). The ERA-interim reanalysis: Configuration and performance of the data assimilation system. *Quarterly Journal of the Royal Meteorological Society*, 137(656), 553–597. <https://doi.org/10.1002/qj.828>
- Deser, C., Lehner, F., Rodgers, K. B., Ault, T., Delworth, T. L., DiNezio, P. N., et al. (2020). Insights from Earth system model initial-condition large ensembles and future prospects. *Nature Climate Change*, 10(4), 277–286. <https://doi.org/10.1038/s41558-020-0731-2>
- Francis, J. A., & Vavrus, S. J. (2012). Evidence linking arctic amplification to extreme weather in mid-latitudes. *Geophysical Research Letters*, 39(6), L06801. <https://doi.org/10.1029/2012GL051000>
- Francis, J. A., & Vavrus, S. J. (2015). Evidence for a Wavier jet stream in response to rapid arctic warming. *Environmental Research Letters*, 10(1), 014005. <https://doi.org/10.1088/1748-9326/10/1/014005>
- Hodges, K. I. (1995). Feature tracking on the unit sphere. *Monthly Weather Review*, 123, 3458–3465.
- Hodges, K. I. (1999). Adaptive constraints for feature tracking. *Monthly Weather Review*, 127(6 II), 1362–1373. [https://doi.org/10.1175/1520-0493\(1999\)127<1362:acft>2.0.co](https://doi.org/10.1175/1520-0493(1999)127<1362:acft>2.0.co)
- Horton, D. E., Johnson, N. C., Deepthi Singh, D. L., Bala Rajaratnam, S., & Diffenbaugh, N. S. (2015). Contribution of changes in atmospheric circulation patterns to extreme temperature trends. *Nature*, 522(7557), 465–469. <https://doi.org/10.1038/nature14550>
- Horton, R. M., Mankin, J. S., Corey, L., Coffel, E., & Raymond, C. (2016). A review of recent advances in research on extreme heat events. *Current Climate Change Reports*, 2(4), 242–259. <https://doi.org/10.1007/s40641-016-0042-x>
- Kornhuber, K., Coumou, D., Vogel, E., Corey, L., Donges, J. F., Lehmann, J., & Horton, R. M. (2020). Amplified rossby waves enhance risk of concurrent heatwaves in major breadbasket regions. *Nature Climate Change*, 10(1), 48–53. <https://doi.org/10.1038/s41558-019-0637-z>
- Kornhuber, K., Petoukhov, V., Petri, S., Rahmstorf, S., & Coumou, D. (2016). Evidence for wave resonance as a key mechanism for generating high-amplitude quasi-stationary waves in boreal summer. *Climate Dynamics*, 49(5–6), 1–19. <https://doi.org/10.1007/s00382-016-3399-6>
- Kornhuber, K., Scott, O., Coumou, D., Petri, S., Petoukhov, V., & Grey, L. (2019). Extreme weather events in early summer 2018 connected by a recurrent hemispheric wave-7 pattern. *Environmental Research Letters*, 14, 054002.
- Lau, W. K. M., & Kim, K.-M. (2012). The 2010 Pakistan flood and Russian heat wave: Teleconnection of hydrometeorological extremes. *Journal of Hydrometeorology*, 13(1), 392–403. <https://doi.org/10.1175/JHM-D-11-016.1>
- Lee, M. H., Lee, S., Song, H. J., & Chang, H. H. (2017). The recent increase in the occurrence of a boreal summer teleconnection and its relationship with temperature extremes. *Journal of Climate*, 30(18), 7493–7504. <https://doi.org/10.1175/JCLI-D-16-0094.1>
- Lee, S. H., Williams, P. D., & Frame, T. H. A. (2019). Increased shear in the North Atlantic upper-level jet stream over the past four decades. *Nature*, 572(7771), 639–642. <https://doi.org/10.1038/s41586-019-1465-z>
- Mann, M. E., Rahmstorf, S., Kornhuber, K., Steinman, B. A., Miller, S. K., Petri, S., & Coumou, D. (2018). Projected changes in persistent extreme summer weather events: The role of quasi-resonant amplification. *Science Advances*, 4, eaat3272.
- Mueller, B., & Sonia, I. S. (2012). Hot days induced by precipitation deficits at the global scale. *Proceedings of the National Academy of Sciences of the United States of America*, 109(31), 12398–12403. <https://doi.org/10.1073/pnas.1204330109>
- Nowack, P., Runge, J., Eyering, V., & Haigh, J. D. (2020). Causal networks for climate model evaluation and constrained projections. *Nature Communications*, 11(1), 1415. <https://doi.org/10.1038/s41467-020-15195-y>
- Overland, J. E., Klaus Dethloff, J. A., Francis, R. J., Hall, E. H., Kim, S.-J., Screen, J. A., et al. (2016). Nonlinear response of mid-latitude weather to the changing arctic. *Nature Climate Change*, 6(11), 992–999. <https://doi.org/10.1038/nclimate3121>
- Perlitz, J., Martin, H., & Randall, D. (2015). Arctic tropospheric warming: causes and linkages to lower latitudes. *Journal of Climate*, 28(6), 2154–2167. <https://doi.org/10.1175/JCLI-D-14-00095.1>
- Pfleiderer, P., & Coumou, D. (2017). Quantification of temperature persistence over the northern hemisphere land-area. *Climate Dynamics*, 51(1–2), 627–637. <https://doi.org/10.1007/s00382-017-3945-x>
- Pfleiderer, P., Schleussner, C. F., Kornhuber, K., & Coumou, D. (2019). Summer weather becomes more persistent in a 2C world. *Nature Climate Change*, 9, 666–671. <https://doi.org/10.1038/s41558-019-0555-0>
- Schiemann, R., Athanasiadis, P., Barriopedro, D., Doblas-Reyes, F., Lohmann, K., Roberts, M. J., et al. (2020). Northern Hemisphere blocking simulation in current climate models: Evaluating progress from the climate model intercomparison project Phase ~5 to 6 and sensitivity to resolution. *Weather and Climate Dynamics*, 1(1), 277–292. <https://doi.org/10.5194/wcd-1-277-2020>
- Screen, J. A., Deser, C., & Simmonds, I. (2012). Local and remote controls on observed arctic warming. *Geophysical Research Letters*, 39(10), L10709. <https://doi.org/10.1029/2012GL051598>

- Screen, J. A., & Simmonds, I. (2010). The central role of diminishing sea ice in recent arctic temperature amplification. *Nature*, 464(7293), 1334–1337. <https://doi.org/10.1038/nature09051>
- Screen, J. A., & Simmonds, I. (2013). Exploring links between arctic amplification and mid-latitude weather. *Geophysical Research Letters*, 40(5), 959–964. <https://doi.org/10.1002/grl.50174>
- Shaw, T. A., & Voigt, A. (2015). Tug of war on summertime circulation between radiative forcing and sea surface warming. *Nature Geoscience*, 8(7), 560–566. <https://doi.org/10.1038/ngeo2449>
- Shepherd, T. G. (2014). Atmospheric circulation as a source of uncertainty in climate change projections. *Nature Geoscience*, 7(10), 703–708. <https://doi.org/10.1038/ngeo2253>
- Shepherd, T. G. (2015). Climate science: The dynamics of temperature extremes. *Nature*, 522(7557), 425–427. <http://dx.doi.org/10.1038/522425a>
- Tamarin-Brodsky, T., Hodges, K., Hoskins, B. J., & Shepherd, T. G. (2019). A dynamical perspective on atmospheric temperature variability and its response to climate change. *Journal of Climate*, 32(6), 1707–1724. <https://doi.org/10.1175/JCLI-D-18-0462.1>
- Tamarin-Brodsky, T., Hodges, K., Hoskins, B. J., & Shepherd, T. G. (2020). Changes in Northern Hemisphere temperature variability shaped by regional warming patterns. *Nature Geoscience*, 13, 414–421. <https://doi.org/10.1038/s41561-020-0576-3>
- Taylor, K. E., Stouffer, R. J., & Meehl, G. A. (2012). An overview of CMIP5 and the experiment design. *Bulletin of the American Meteorological Society*, 93(4), 485–498. <https://doi.org/10.1175/BAMS-D-11-00094.1>
- Vallis, G. K. (2006). *Atmospheric and ocean fluid dynamics* (11th ed.). Cambridge, UK: Cambridge University Press.
- Wills, R. C. J., White, R. H., & Levine, X. J. (2019). Northern Hemisphere stationary waves in a changing climate. *Current Climate Change Reports*, 5(4), 372–389. <https://doi.org/10.1007/s40641-019-00147-6>
- Yin, J. H. (2005). A consistent poleward shift of the storm tracks in simulations of 21st century climate. *Geophysical Research Letters*, 32(18), L18701. <https://doi.org/10.1029/2005GL023684>
- Zappa, G., & Shepherd, T. G. (2017). Storylines of atmospheric circulation change for european regional climate impact assessment. *Journal of Climate*, 30(16), 6561–6177. <https://doi.org/10.1175/JCLI-D-16-0807.1>